Rock Mech. Rock Engng. (2006) 39 (4), 359–382
DOI 10.1007/s00603-005-0073-4

Rock Mechanics and Rock Engineering
Printed in Austria

A Practical Procedure for the Measurement of Fragmentation by Blasting by Image Analysis

By

J. A. Sanchidrián[1], **P. Segarra,** and **L. M. López**

E.T.S.I. Minas, Universidad Politécnica de Madrid, Madrid, Spain

Received February 3, 2005; accepted April 14, 2005
Published online November 21, 2005

Summary

The operation of a digital image analysis system in a limestone quarry is described. The calibration of the system, required in order to obtain moderately reliable fragmentation values, is done from muckpile sieving data by tuning the image analysis software settings so that the fragmentation curve obtained matches as close as possible the sieving. The sieving data have also been used to extend the fragment size distribution curves measured to sizes below the system's optical resolution and to process the results in terms of fragmented rock, discounting the material coming from a loose overburden (natural fines) that is cast together with the fragmented rock. Automatic and manual operation modes of the image analysis are compared. The total fragmentation of a blast is obtained from the analysis of twenty photographs; a criterion for the elimination of outlier photographs has been adopted using a robust statistic. The limitations of the measurement system due to sampling, image processing and fines corrections are discussed and the errors estimated whenever possible. An analysis of consistency of the results based on the known amount of natural fines is made. Blasts with large differences in the amount of fines require a differentiated treatment, as the fine sizes tend to be the more underestimated in the image analysis as they become more abundant; this has been accomplished by means of a variable fines adjustment factor. Despite of the unavoidable errors and the large dispersion always associated with large-scale rock blasting data, the system is sensitive to relative changes in fragmentation.

Keywords: Rock blasting, fragmentation, image analysis, fines, size distribution, outliers.

1. Introduction

Fragmentation is a key factor in order to control and minimize the loading, hauling, crushing, classification and processing costs in aggregate and industrial minerals operations. The evaluation of the fragmentation of the run of mine by sieving is generally not possible due to its high cost and the disruption it causes in the production cycle. Several alternative procedures can be used to measure fragmentation, such as

belt scale readings in selected positions of the processing plant, production data of the various size fractions, or digital image analysis. The selection of the fragmentation monitoring system is to a large extent site-dependent and the features of the crushing circuit must be considered.

Digital image software was developed through the 1990s and at present it is a worldwide accepted tool in the mining and mineral processing industries. Its main advantage is that it can be used on a continuous basis without affecting the production cycle, which makes it the only practical tool for evaluating fragmentation of the run of mine, despite of its inherent limitations; a thorough discussion of such systems was published by Maerz and Zhou (2003). Some of the errors of image analysis systems can be overcome to some extent by means of an on-site calibration from sieving data, as Latham et al. (2003) suggest for industrial applications. This is not a difficult task for material in a conveyor belt but is problematic for the run of mine in a muckpile. Ouchterlony (2003) makes an excellent revision of digital image analysis methods.

A continuous fragmentation monitoring system was installed in El Alto quarry (Spain) with the aim of controlling fragmentation by blasting as a means to improve the overall operation. The system works successfully from February 2002 and the images are processed with the digital image analysis software *Split*® (Split Engineering, 2001; Kemeny et al., 1999). This paper describes the tuning of the fragmentation monitoring system installed at El Alto and the procedure developed for measuring the fragmentation by blasting. This task was undertaken as preliminary for a long-term goal of developing a fragmentation prediction model for El Alto.

2. The Quarry and the Measurement System

El Alto quarry is located in the province of Madrid, Spain; 2.25 Mt/yr of limestone and clayish marl are mined for cement manufacture in the plant adjacent to the quarry. The deposit is of Tertiary age and lacustrine origin. The geology in El Alto is simple and essentially uniform. In the upper four to six meters there is an overburden of clayish marl of sandy nature and little cohesion. In the floor of the limestone there is clay (*greda*), which is not mined. The limestone pack has a thickness of 12 to 19 m and is located between the marl overburden and the *greda* floor; it is almost horizontal and crossed by different sets of joints and discontinuities.

The quarry is mined in one bench. The overburden material, which we refer to as ''natural fines'', is included in the blast, which complicates the fragmentation measurements. The amount of these natural fines is estimated as the ratio of the overburden thickness to the bench height; it varies from 9 to 45%, with typical values around 25%.

The crushing process consists of a primary, hammer mill, with a bottom screen of 65 mm opening, followed by a vertical axis roller mill. This mill grinds and blends the limestone and the marl – plus additives – to form the powder-like kiln feed, which is conveyed to homogenizing silos where the powder is analyzed and further treated prior to being fired in the kiln. The fragment size of the blasted material affects to the consumables of loaders, shovels and trucks, the loading cycle and the mill's energy consumption and throughput. The last is also affected by $P_{63\,\mathrm{mm}}$ (fraction passing at

63 mm) since the fines material tend to block the screen, especially in rainy conditions, due to caking.

Fragmentation measurements may be done in a variety of locations depending on the intended use of the fragmentation control. If the purpose is blasting control, measurements in the processing plant, after the primary crusher, make it difficult to relate with fragmentation in the muckpile and cannot be used to assess the influence of blast design on fragmentation. Given this, a suitable option is to measure fragmentation in the hopper of the primary crusher. Another convenient measuring position before the primary crusher is on the top of the trucks, but this was thought to be less appropriate than the hopper, since the fines are more segregated during the truck run from the pit to the mill. In both cases, fragments larger than about 1 m^3 are excluded from the fragmentation measurements, as they are not hauled to the crusher until they have been secondarily fragmented. Direct measurements on the muckpile were found to be impossible to carry out on a systematic basis.

The monitoring system installed at El Alto is formed by a video camera, a trigger, a set of lights, a PC installed in the control room of the crushing station and a connection between the camera and the PC. The camera is above the primary crusher's hopper, 6.5 m from the surface of the material to be analyzed, when the bin is full; the set-up is shown in Fig. 1. The resolution of the camera for this set-up is 50 mm (Tessier et al., 2002).

Normally, more than one blast is loaded at the same time. In order to assign the photographs to the respective blast, a color is associated to every blast. Software installed in the computer of the control room shows the trucks that are currently working and the blasts that are being loaded – represented by their color and identi-

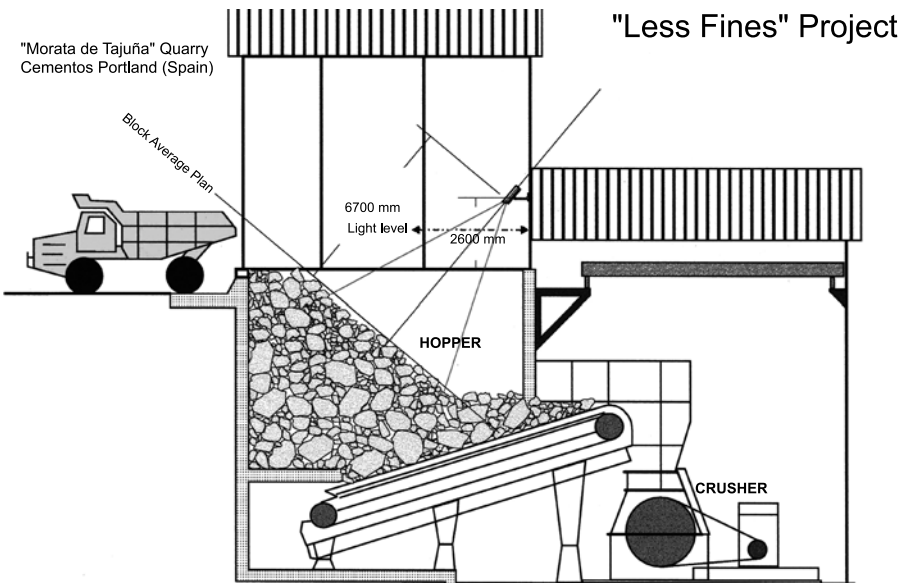

Fig. 1. Camera set-up installed in the primary crusher building in El Alto (Tessier et al., 2002)

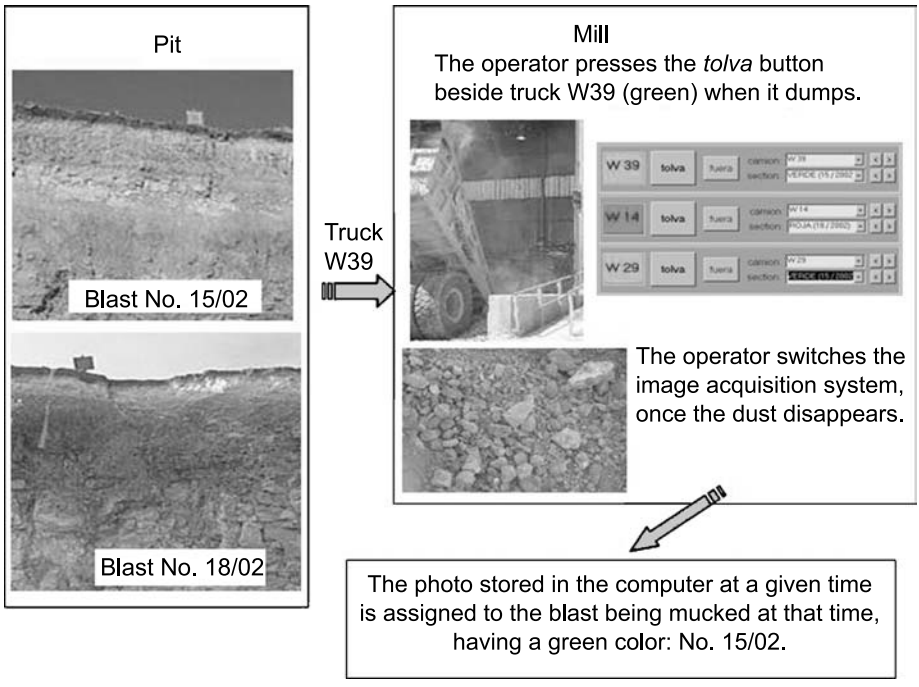

Fig. 2. Working procedure for the photographs' assignment to blasts in El Alto

fication number. The working procedure is shown graphically in Fig. 2. A color is assigned to each blast from the time the block is drilled until the muckpile is completely loaded; a flag of this color is allocated in the highwall crest. At the beginning of the shift, the crusher operator enters the identification numbers of the blasts being mucked and their colors in the computer, and the trucks are assigned to the different blasts (trucks load from a unique muckpile during the whole shift and they carry in the front a flag of the color of the blast they are currently hauling). The screen in the computer looks then like that shown in Fig. 2, with the truck identification and the color of the blast it is currently hauling. When a truck dumps, the mill operator presses the button that refers to the truck; once the conditions are favorable for a good quality image (settlement of the dust), the operator triggers the camera. The resulting photo is stored in the PC. A data base links the computer time at which each photo was made with the dumping time – which differ by a lapse of some seconds – and the color, so that the origin of the material is known: the blast of that color being loaded at that time.

3. Calibration of the Digital Image Analysis Software

The images are processed with the digital image analysis software *Split® Desktop*. This section describes the tests made in order to assess and optimize the performance of the software. These tests were relevant in developing the methodology that is described in Section 4.

3.1. Performance of the Image Analysis Software in Automatic Mode

Split can function in automatic or manual modes, or a combination of both (auto & manual). In the latter, the operator uses the automatic delineation done by the code and corrects the errors visually. The correction process can be very time-consuming. A test to check the performance in automatic mode (obviously advantageous from an economic standpoint), without corrections, versus the auto & manual mode was done on a conveyor belt. The belt conveying material from the outlet of the hammer mill was used for this purpose; the belt was stopped and a photograph was taken of the material on it (Fig. 3). A sample of about 60 cm in length was taken from the photographed area of the belt, for further laboratory standard screening. This sampling procedure was considered enough for our purposes – a more involved method for making belt-cuts, sieving and calibrating the system is given by Kemeny et al. (1999). The photograph was analyzed with *Split* in both automatic and auto & manual modes; the fines adjustment factor – a calibration parameter that, roughly, accounts for the material smaller than the resolution of the image, ''fines'' (Split Engineering, 2001; Kemeny et al., 1999) – was given the value 100% in both analyses (the fines factor can be less than 100%, if the fines are overrated, or greater, if the fines are hidden). The ''autofines'' option – that enables the automatic detection of the fines patches – was activated in the automatic mode.

The actual fragmentation of the material on the belt, obtained by sieving, and the size distribution curves from *Split*-automatic and *Split*-auto & manual are plotted in Fig. 4. The size distribution curve given by *Split* in auto & manual mode is quite close to the one obtained by sieving, while the one given by *Split* in automatic mode is well below. Maerz and Zhou (1998), working with the image analysis code *Wipfrag*, mention that particles with different textures and grey densities – clayish-marl's fines patches appear between the limestone fragments – tend to confuse the delineation. In fact, the automatic delineation incurs in certain errors, sometimes quite significant, especially in the detection of the fines patches that are often confused with rock fragments. This leads to an overestimation of the sizes when the automatic delineation

Fig. 3. Photograph of the material carried by the conveyor belt

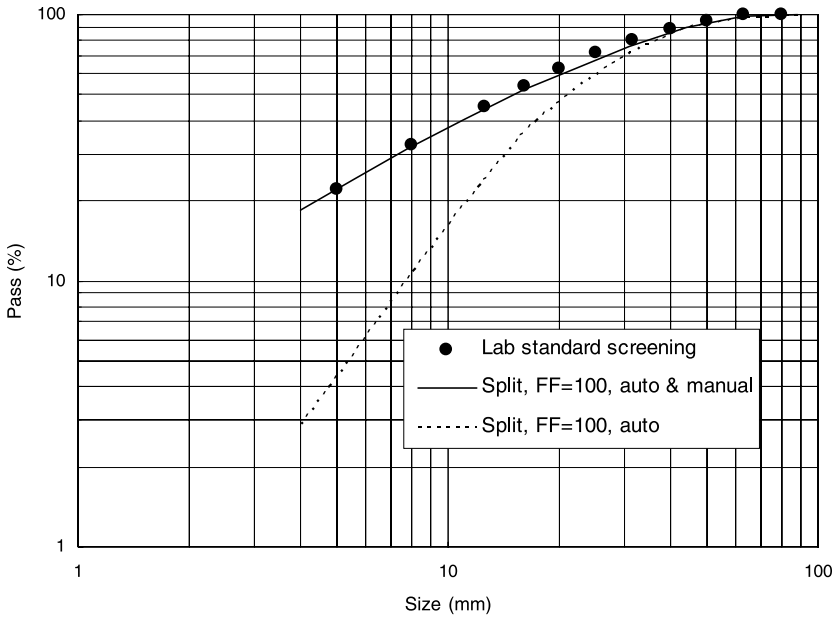

Fig. 4. Size distribution curves for material in the belt obtained by sieving and with *Split*

is not corrected, resulting in larger median size and more uniform distribution, and fewer fines than actual.

The errors made in the automatic mode can thus be attributed to the system's ability for delineating the particles, allocating particles to size ranges, and recognizing and treating the fines.

3.2. Calibration of the System. Muckpile Sieving

As shown in the preceding section, the manual correction of the automatic delineation is required in order to have reliable fragmentation results. Besides this, the fines factor must be calibrated from sieving data. This can be easily done for the material on a belt, but such calibration would be useless for the material in the hopper of the crusher, as its topology is very different. For the calibration of the fines factor in photographs at the hopper, a sample of a blast was sieved, the resulting fractions were homogenized, and then loaded into the primary crusher, where photographs were taken.

Production blast no. 10/03 was selected for this purpose. A cut perpendicular to the face was opened in the muckpile with a Cat 992 front-end loader in order to collect material ranging from the highwall face to the opposite end of the muckpile – about 30 m away from the wall. The loader moved its bucket from bottom to top, taking material across the vertical of the pile. This sampling procedure allowed taking a representative sample, with material coming from both the heart of the blast and from the overburden. The sampled material was stocked in a new pile from which an excavator fed it to a mobile *Powerscreen Turbo Chieftain 1400* (see Fig. 5).

Fig. 5. General view of the mobile screen, front loader, excavator and piles

The mobile screen had three screens of sizes 90/110 mm, 46/48 mm and 20 mm. The first screen was formed by non-parallel rods separated 90 mm in one side and 110 mm in the opposite side. The second screen had rectangular openings of 48×46 mm. Screen openings were measured on-site. Fragments exceeding the excavator's capacity (larger than about 800 mm) were not fed onto the screen. Four fractions: 800–110, 110–48, 48–20 and <20 mm were thus obtained.

The piles relative to each fraction were loaded into trucks equipped with on-board scales. A negligible amount of material was lost in this operation. The mass of each fraction and the cumulative pass percentages are given in Table 1. A sample of the fine fraction was screened in the laboratory, with the aim to extend the size distribution down to 0.063 mm. The cumulative pass is shown in Table 2. The total fragment size distribution from the sieving is shown in Fig. 6. A pile was then rebuilt from the individual screening piles, homogenized, loaded into trucks and dumped to the primary crusher. A total of four photos of this material were taken in the hopper and the fragmentation determined with *Split*. These photos are shown in Fig. 7.

A constant density for all size fractions has been assumed, so that the size distribution curves given by Split (which are volume-based) and the one obtained by sieving

Table 1. Fragmentation data of the run of mine obtained by sieving

Size class (mm)	Mass (t)	Size (mm)	Cumulative pass (%)
800–110	205	800	100
110–48	103	110	57.4
48–20	47	48	36.0
<20	126	20	26.2
Total	481	–	–

Table 2. Size distribution of a sample of the muckpile fraction <20 mm

Sieve size, mm	20	14	12.5	10	6.3	4	2	1	0.5	0.25	0.125	0.1	0.063
Pass, %	100	90.9	85.5	76.6	62.4	50.8	34.0	21.4	12.1	6.5	3.2	2.49	1.36

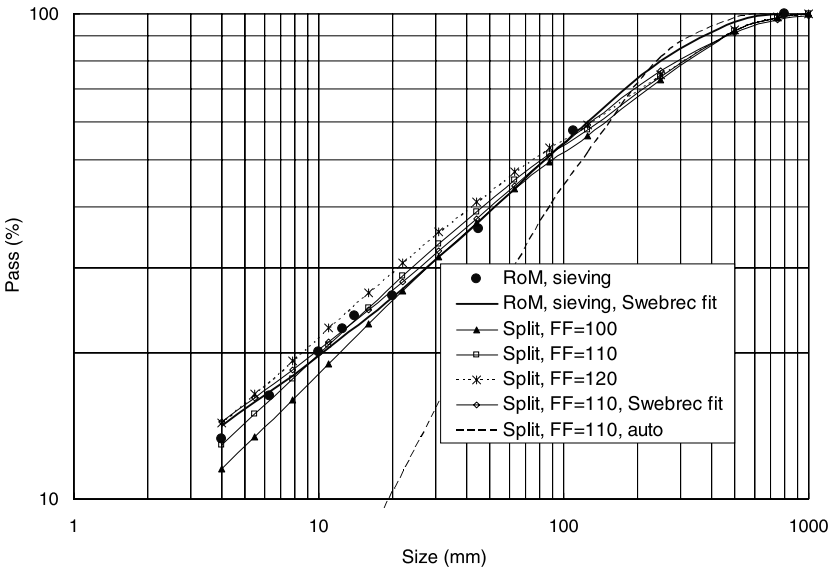

Fig. 6. Adjustment of the fines correction factor

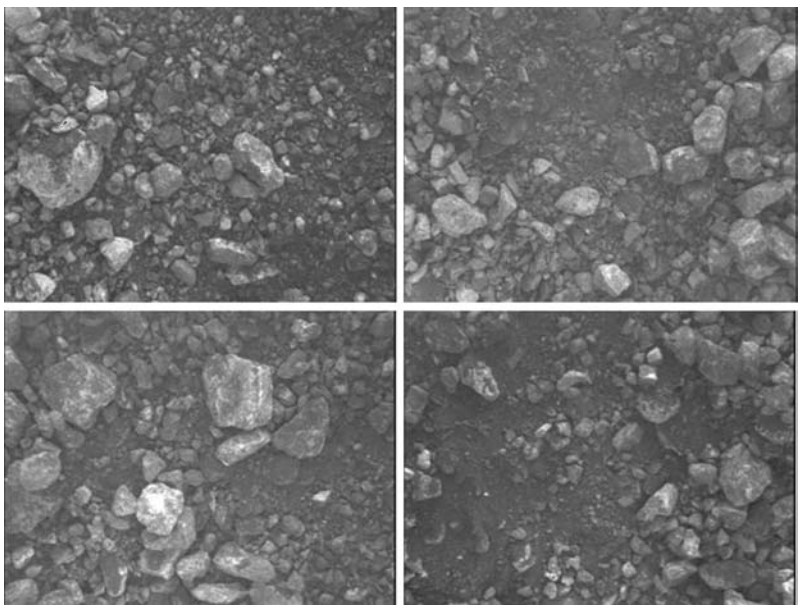

Fig. 7. Photographs analyzed from the material sieved in the calibration test

(mass-based) are directly compared. The four binary images were analyzed in auto & manual mode. The ''best fit'' option was selected for the fines distribution, which means that the software uses the distribution, Schuhmann or Rosin-Rammler, which

works better (Split Engineering, 2001). The manual analysis was done by two different persons and the average curve was calculated. Different fines factors were used.

The *Split* data points and the sieving points have different abscissa values; in order to assess the differences of both size distributions, the Swebrec function (Ouchterlony, 2005) was fitted to the points from the sieving down to 4 mm, the minimum size given by *Split*; this fitting provides a very good description of the existing data points ($R^2 = 0.998$), as can be seen in Fig. 6. The root mean squared relative differences between the sieved-Swebrec values and the *Split* values from 750 mm down to 4 mm (14 points) were 0.134, 0.081, 0.050 and 0.081 for fines correction factors 130, 120, 110 and 100, respectively. A factor of 110% was thus chosen. Figure 6 shows the *Split* curves for fines factors 100, 110 and 120. It should be noted that the *Split* curves separate significantly from the Swebrec fit in the coarse region; this is due to the fact that the zone between 110 and 800 mm is unresolved in the muckpile screening. If a Swebrec function is newly fitted to the best *Split* curve (fines factor 110) down to 4 mm, the goodness of the fit is again remarkable ($R^2 = 0.998$). Figure 6 also shows the *Split* curve for FF = 110 in automatic mode, illustrating the bad results with this option, as discussed in Section 3.1.

4. Method for the Determination of Fragmentation

The basics steps, once the photographs from a blast are available, are: sampling of the photos, processing the images with *Split*, obtaining the size distribution curve of the blast and subtracting the contribution of the overburden material.

4.1. Photo Sampling

The photos are randomly sampled from the whole set of images assigned to a blast. Photos with bad quality, poor or uneven lighting, or partially empty bin (this has an influence on the distance between the camera and the material, hence on the scale of the image), are rejected manually. In some blasts, more than half of the photographs are eliminated with these criteria.

At least twenty photos per blast are selected for the analysis. However, if some of the images sampled are not representative of the fragmentation of the blast (details on this are given in Section 4.3), additional ones are sampled until a minimum of 20 representative images are obtained.

The size of the sample used is a compromise between the available resources (time spent in the manual editing of the images) and the requirement for the set of images to be representative of the whole blast. Assuming a standard deviation for a parameter (e.g. x_{50}) 25% of the mean value, twenty images result in a confidence interval at a 95% significance level of 16% of the mean. The confidence interval would be smaller if a greater number of photos per blast were analyzed.

4.2. Scaling, Automatic Delineation and Manual Editing

The scale of the photograph is known from the camera opening and the distance to the rock surface (see Fig. 1), which is approximately perpendicular to the camera's optical

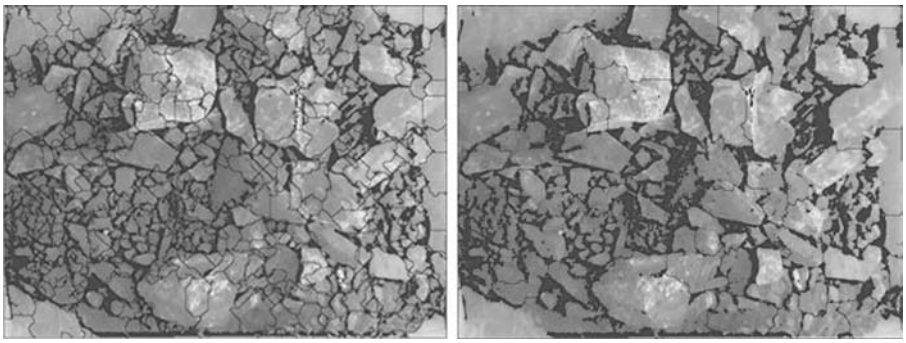

Fig. 8. Auto-delineations made with the delineations parameters set to (**a**) minimum and (**b**) maximum

axis. The resolution of the camera in the present case is 5.4 mm/pixel and the height of the photo is 576 pixels.

The ''autofines'' option is switched off in the automatic delineation menu, as large errors are committed using it. According to Norton (2003), a proper delineation should be made in this stage in order to reduce the required amount of editing. For this purpose, the three delineation parameters – noise size, watershed ratio and gradient ratio (Split Engineering, 2001) – are modified and set conveniently according to the characteristics of the photograph (lighting, contrast, dust, etc.) and the user's experience until the delineation is, in principle, acceptable. As an example, Fig. 8 shows two automatic delineations of the same photo with different settings of the values of the delineation parameters.

The manual editing is focused in the main errors of the automatic delineation. This consists of correcting the over-divided large rocks and marking the fines' areas, which are the main causes of the tendency of digital image analysis software to give more uniform distributions (Ouchterlony, 2003). Many of the smaller particles, whose delineated edges are not modified, are under the maximum size of fines – called fines cut-off and obtained from the peak or peaks of the histogram of volume of particles (Split Engineering, 2001; Kemeny et al., 1999) – and they will be included in the fines estimation. The software calculates the total area of fines from the sum of the areas of the particles smaller than the fines cut-off and the product of the fines patches' area times the fines adjustment factor.

This quick manual editing leads to a slightly different size distribution curve than if a very detailed editing, particle by particle, of the automatic delineation were made (see Section 5.2), but it is much more time-efficient.

4.3. Calculation of the Size Distribution Curves of Each Image and of the Blast

The size distribution for each single image is calculated using the fines adjustment factor determined in the calibration test, 110%, and the ''*best fit*'' option activated. The time spent per photo in the analysis is about 20 minutes, most of the time being dedicated to correct the automatic delineation.

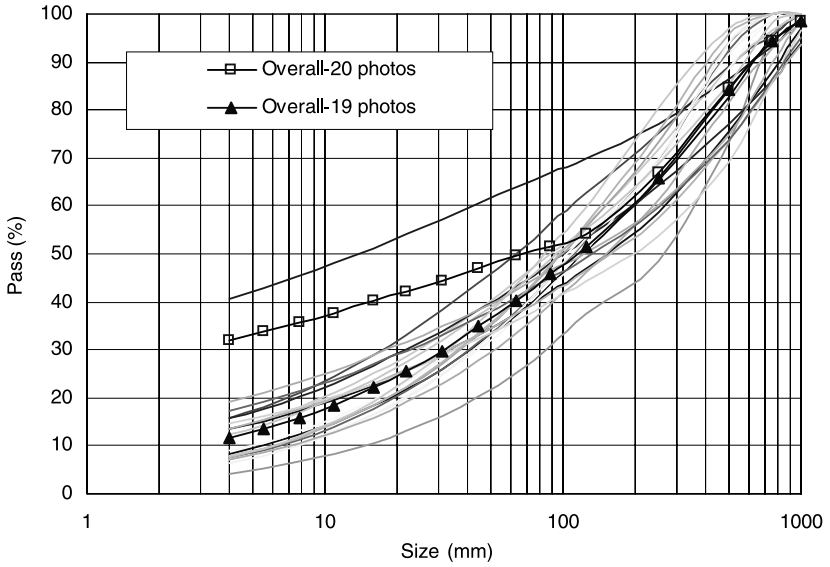

Fig. 9. Influence of outlier curves on the overall fragmentation

Most of the size distribution curves of the twenty photos of a blast form a fairly tight package. However, sometimes a few curves have a different slope and lie clearly outside that bundle. This is illustrated in Fig. 9, where one curve of the twenty photos analyzed is very different to the others, with a very small median size. This curve relates to a photograph with few fragments and with most of the surface covered with fines patches. The opposite case (photos with very large fragments and few fines) does also happen. Other cases of bad photographs, such as half-empty hopper, bad illumination, shadows, etc., are directly rejected (as explained in Section 4.1) before the digital analysis is carried out.

The identification of outlying curves is done assuming that the distribution of medians (x_{50}) is log-normal, which can be confirmed by a goodness-of-fit test to the log-normal fit of the set of medians of many blasts (this could be expected, as the individual size distributions from each photograph can themselves be acceptably described as log-normal). The median absolute deviation about the median (*MAD*) has been used as robust variance estimator (Rousseeuw and Leroy, 1987):

$$MAD = \text{median}\{|\ln x_{50i} - \text{median}(\ln x_{50i})|\}. \tag{1}$$

And the deviations relative to the *MAD* are calculated as:

$$Z_i = \frac{|\ln x_{50i} - \text{median}(\ln x_{50i})|}{MAD}. \tag{2}$$

The individual curves are rejected when $Z_i \geq 5$ (Miller and Miller, 2000).

A new photograph is analyzed whenever one photograph has been taken out as outlier, so that 20 valid photographs are always used for making up the fragmentation curve of the blast (unless the total number of valid photographs is less than 20, a very rare case).

4.4. Calculation of the Size Distribution Curve of the Fragmented Limestone

The overburden, whose thickness varies from blast to blast, contributes to the fines in the muckpile. In order to get the actual fragmentation produced by blasting, the loose overburden has to be discounted from the raw data given by *Split*. For this purpose, a representative sample of the overburden was collected and the size distribution obtained by standard sieving; this is given in Table 3.

For sizes larger than or equal to 14 mm (maximum size of the overburden), the size distribution $P_L(x)$ of the fragmented limestone is as follows:

$$P_L(x) = 100 \cdot \frac{P(x) - NF}{100 - NF}, \tag{3}$$

where $P(x)$ is the cumulative pass given by *Split* for a size x and NF is the natural fines fraction present in the block.

For sizes smaller than 14 mm, the size distribution of the fragmented rock is obtained from the muckpile and the overburden sieving data. The cumulative size distribution of the muckpile below 14 mm for the blast sieved can be obtained from Table 2 by normalizing with respect to the passing at 14 mm (90.9%); it is given in Table 3. The classes for each size interval are formed from these; let f_{Mi} and f_{OBi} be the

Table 3. Size distribution of a sample of the overburden and of the muckpile below 14 mm

Sieve size (mm)	14	12.5	10	6.3	4	2	1	0.5	0.25	0.125	0.1	0.063
Pass, overburden (%)	100.0	96.8	93.3	79.3	71.4	55.8	42.1	24.1	14.0	7.7	5.8	3.3
Pass, muckpile (%)	100.0	94.0	84.3	68.6	55.9	37.4	23.5	13.3	7.2	3.5	2.7	1.5

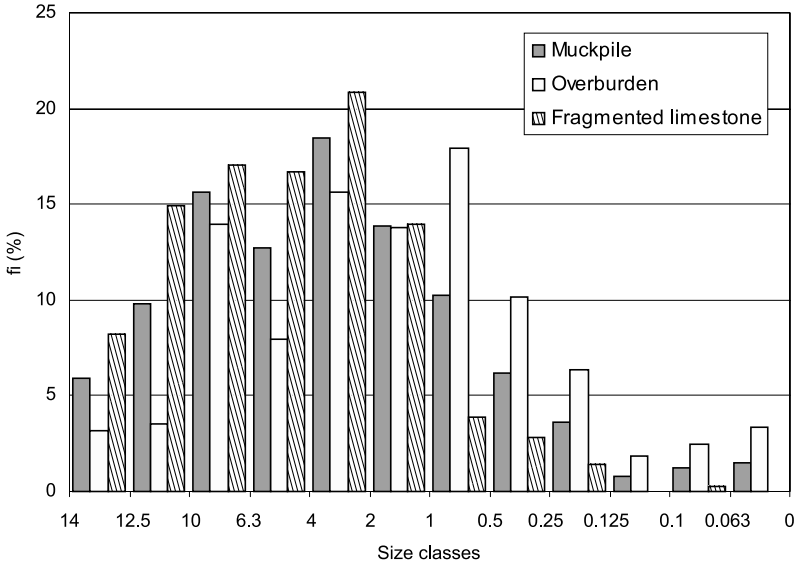

Fig. 10. Histograms of the overburden and the muckpile below 14 mm

Table 4. Size distribution below 14 mm, $P_{L-14}(x)$, of the fragmented rock

Sieve size, mm	14	12.5	10	6.3	4	2	1	0.5	0.25	0.125	0.1	0.063
Pass, %	100.0	91.8	76.8	59.8	43.1	22.3	8.3	4.5	1.6	0.2	0.0	0.0

percentages of each class in the muckpile and in the overburden, respectively (from the total material below 14 mm); they are shown in Fig. 10.

Let the total mass of material in the muckpile be M; the mass of a class i is:

$$m_{Mi} = M \frac{P_{14\,\mathrm{mm}}}{100} \frac{f_{Mi}}{100}. \tag{4}$$

$P_{14\,\mathrm{mm}}$ [$\equiv P(x = 14\,\mathrm{mm})$] being the fraction (percentage) of material below 14 mm in the muckpile, from the *Split* analysis. The mass of the same class originally in the overburden is:

$$m_{OBi} = M \frac{NF}{100} \frac{f_{OBi}}{100}. \tag{5}$$

And the mass of class i in the fragmented limestone is:

$$m_{Li} = m_{Mi} - m_{OBi}. \tag{6}$$

The frequency (percent) of the classes in the fragmented limestone are, relative to the material below 14 mm:

$$f_{Li} = 100 \frac{m_{Li}}{\sum_{i=1}^{z} m_{Li}} = \frac{P_{14\,\mathrm{mm}} f_{Mi} - NF\, f_{OBi}}{P_{14\,\mathrm{mm}} - NF}. \tag{7}$$

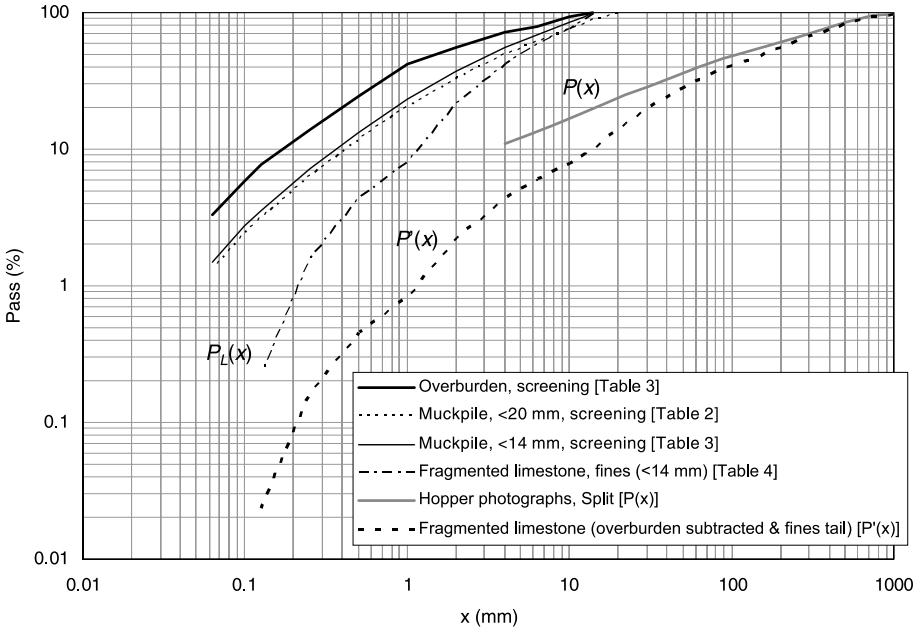

Fig. 11. Size distributions in the derivation of the fragmentation of the limestone

These are shown in Fig. 10 (in the blast sieved, $NF = 10.8\%$). The cumulative size distribution below 14 mm (the limestone fines), $P_{L-14}(x)$, formed from f_{Li} is shown in Table 4; $P_{L-14}(x = 14\,\text{mm})$ is obviously 100%.

Moser et al. (2000) and Moser (2003) show a strong similarity between the shape of the finer part of the size distribution curves of a given rock type, irrespective of the fragmentation process applied, either mechanical comminution or blasting. From this, it is suggested that the fines tail of the size distribution curve is essentially a characteristic of the rock. Assuming that this holds true for the fragmented rock in El Alto, the size distribution curve for the fragmented limestone below 14 mm obtained for the blast that was sieved, shown in Table 4, is also used for all the other blasts. This fines tail is linked at 14 mm:

$$P_L(x) = P_L(x = 14)\frac{P_{L-14}(x)}{100}. \tag{8}$$

Figure 11 shows the various size distribution curves of the correction process.

5. Sources of Error

The limitations of the fragmentation monitoring system encompass different errors that may affect its reliability and hinder its use for fragmentation control. Errors can be grouped into three categories, namely:

- from the sampling method,
- from the image analysis process, and
- from the method of subtracting the natural fines.

5.1. Errors due to Sampling

A first limitation comes from the requirement of the photographs to be representative of all the rock fragments. In most blasts, the 20 photos analyzed represent about a 12% of the muckpile material. Forty photographs from one blast were chosen and processed; groups of 20, 10, 5, 2 and 1 photos were randomly formed from those. This arrangement was done twice (samplings a and b). The respective size distribution curves of the RoM are plotted in Fig. 12. The Swebrec size distribution function (Ouchterlony, 2005) was fitted to them; the characteristic Swebrec parameters: maximum size, $x_{\max}$, mean size, x_{50} and undulation parameter, b together with the correlation factor are listed in Table 5. The correlation factor is quite good in all the cases; it is at least 99.8%. The errors in x_{50} and b with respect to the fragmentation data obtained with the complete set of 40 photos – considered to be the best approach to the actual fragmentation of the muckpile – are shown in Table 5; $x_{\max}$ is about the nominal maximum size loaded into the primary and is not considered in the analysis ($x_{\max}$ was restricted in the fittings to be greater than or equal to 1000 mm). If 20 photos are considered, the agreement with the 40 photos' size distribution curve is good (the errors are within 7%). If less than 10 photos are considered, the errors may increase strongly, especially in x_{50}.

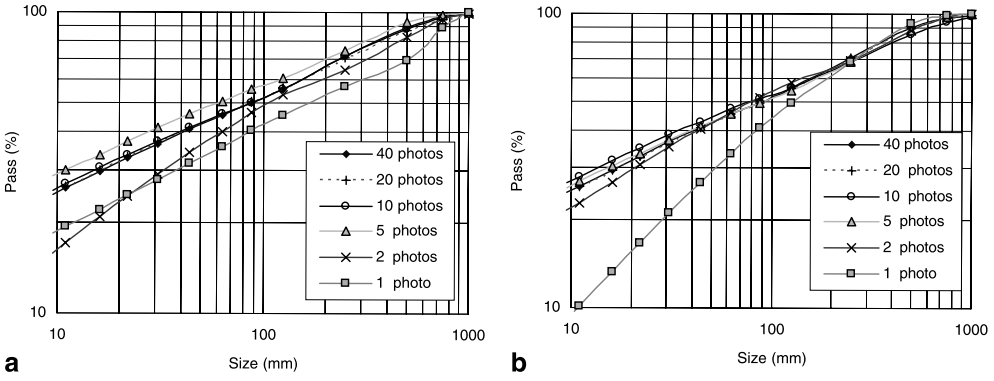

Fig. 12. Size distribution curves of RoM for two analyses (**a**) and (**b**) for different numbers of photographs

Table 5. Swebrec parameters, correlation factor and errors committed for different samples of photos

Sample size	Sample	x_{max} (mm)	x_{50} (mm)	b	R^2 (%)	Errors (%)	
						x_{50}	b
40	–	1000	87	1.62	99.9	–	–
20	(a)	1253	83	1.71	99.9	4	−6
	(b)	1127	85	1.73	99.9	3	−7
10	(a)	1116	85	1.67	99.9	2	−3
	(b)	1137	79	1.43	99.9	9	12
5	(a)	1000	62	1.66	99.8	28	−2
	(b)	1000	89	1.50	99.8	−2	8
2	(a)	1070	118	1.53	100.0	−36	5
	(b)	1000	83	1.55	99.8	5	4
1	(a)	1006	189	1.11	99.6	−118	32
	(b)	1000	131	2.21	99.9	−51	−36

5.2. Errors due to the Image Processing

The calibration of the system was done from the comparison of optic and sieving measurements, each with its own limitations. For instance, optical systems measure the long and intermediate diameters of the fragments while the intermediate and small diameters are measured when the material is sieved (Maerz and Zhou, 1998); additionally, the errors inherent to a 2D analysis, like the fragments overlapping, are not present when a sample is sieved.

The required manual editing is a new source of errors. A test was carried out in which a very detailed editing (particle by particle, of about two hours), and a quick one (as described in Section 4.2) were done on two photos (A and B). The size distribution curves for both the detailed and the ''time optimized'' analyses are shown for each photo in Fig. 13; the differences in pass increase as the size decreases; in $P_{63\,mm}$ they are about 3%, while the differences in $P_{4\,mm}$ are 10 and 27%. The latter is rather large, but 4 mm is anyway far below the optical resolution of the system (50 mm).

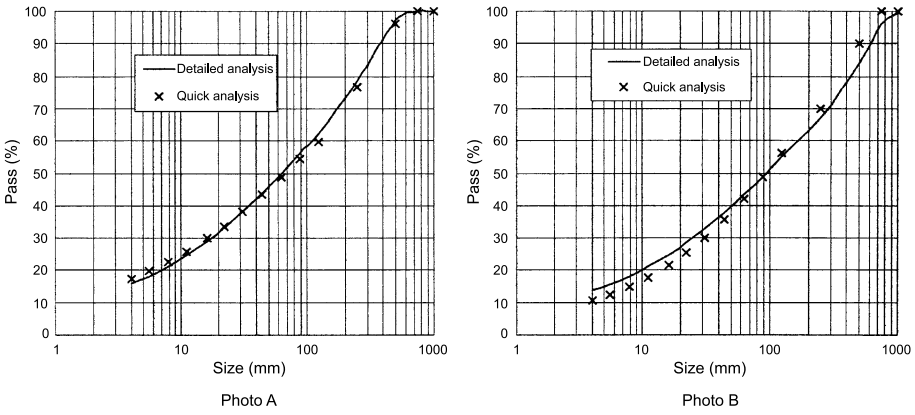

Fig. 13. Analysis of two photos; results with detailed and quick analyses

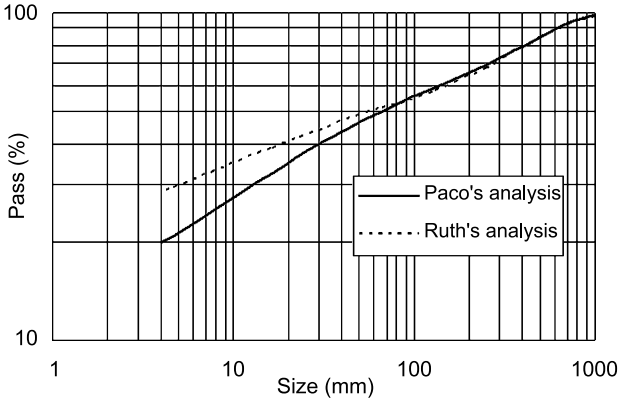

Fig. 14. Analysis of a blast (20 photographs) by two users

The unavoidable manual editing of the photographs encompasses some subjectivity. Figure 14 shows the size distribution curves from the analysis of the same set of twenty photographs from a blast made by two operators. The resulting fragmentation is very similar for sizes larger than 88 mm. The fines cut-off of the photographs in Fig. 14 is 100 and 78 mm. So, the manual corrections seem to be relatively independent of the user at sizes larger than the fines cut-off. Below that size, the curves clearly diverge; the relative errors at 63 mm (the last point above the camera resolution limit) are still low, 4%, while they become important, 45%, at 4 mm. It is clear that the precise identification and delineation of patches of fines and fine particles is difficult not only for the image analysis software but also for the human eye.

The muckpile in El Alto is formed by broken limestone and natural fines. When the amount of natural fines is high, either the coarse particles may be hidden by the fines spread all over the surface, causing an overrepresentation of fines, or it may also happen that the fines are segregated underneath the material's surface, resulting in an

underestimate of their amount. If the amount of natural fines is small, the surface view may represent fairly well the material below. As Latham et al. (2003) state, the fines adjustment factor is not expected to account for the unpredictable effects of gravity segregation. As both of the above situations (large and small amount of fines) may take place in photographs of the same blast, several calibration tests with material coming from different types of size distributions would be required. A variable fines adjustment factor would then be used depending on the topology of the photograph. This however would complicate the process and would probably bring about more subjectivity into it. This matter is revisited from a different standpoint in Section 6.

5.3. Errors due to Subtracting the Natural Fines

The correction for natural fines is probably a new source of error. Firstly, the estimation of the amount of natural fines present in the block is based on a plane section of the block blasted (the highwall face). Secondly, the maximum size of the natural fines, 14 mm, obtained from only one sample, may be subject to changes across the quarry. Finally, the *Split* passing at 14 mm is a weak point, as it is well in the range where errors of the measurements are relatively important, as Figs. 13 and 14 show.

6. Discussion

The sieving of blast 10/03 shows that the muckpile's size distribution curve given by *Split* from photographs at the primary crusher feed can acceptably match the measured one (see Fig. 6), but it is not possible to check the accuracy of the system in each particular blast. For most applications related with fragmentation by blasting, however, it may be enough if the system is able to respond to changes in the fragmentation consistently.

The fragmentation values of 35 blasts for which the blasting parameters were carefully measured were determined following the methodology described above. The blasts were done with different explosives, hole diameter, drilling pattern, powder factor, initiation system and interhole delay. Some fragment size characteristic values of the run of mine (80%, 50% and 20% passing sizes, and the percentages passing at 14, 63 and 250 mm) are given in Table 6, together with the fraction of natural fines of each blast.

The blasting with an overburden of fine material brings a good way to assess the consistency of the measurements: fragment sizes in the muckpile at a given percentage passing should in general be finer when the amount of natural fines is high, or the fractions passing at a given mesh size should be higher. Figure 15 shows the 80, 50 and 20% passing sizes as a function of the natural fines. They all decrease as the natural fines increase; linear fits (not straight lines due to the logarithmic ordinate) are plotted. The scatter in the data (large in general due to the uncontrollable factors usually encountered in production blasts and, in the present case, also to the variability of the blasting parameters) is larger as the size gets smaller. The fines cut-off value for all photographs analyzed ranged from 52 to 108 mm with a mean value of 82 mm and a standard deviation of 16 mm.

Table 6. Fragmentation values

Blast #	*NF* %	x_{80} mm	x_{50} mm	x_{20} mm	$P_{14\,mm}$ %	$P_{63\,mm}$ %	$P_{250\,mm}$ %
1	15.3	383.1	103.3	12.3	21.3	42.2	68.0
2	17.1	382.1	95.3	10.2	22.9	42.8	68.7
3	12.3	442.8	103.7	10.8	22.6	42.2	65.2
4	40.8	277.8	32.6	2.1	41.0	57.5	77.9
5	29.9	423.6	67.0	2.1	37.6	49.5	66.2
6	24.0	334.2	64.7	3.7	30.7	49.6	72.9
7	12.1	390.1	81.8	4.6	29.0	46.9	68.9
8	22.9	338.0	46.6	2.4	36.8	53.5	73.1
9	10.8	417.6	119.8	14.8	19.5	39.3	65.7
10	34.7	317.0	50.6	4.9	30.9	53.7	75.2
11	9.7	368.0	89.1	2.4	34.1	46.6	70.3
12	9.9	417.9	77.7	10.0	23.7	47.0	68.1
13	40.2	328.3	22.7	1.6	46.6	57.9	74.8
14	14.1	350.8	79.3	6.7	26.6	46.3	71.1
15	24.4	364.6	87.3	8.5	24.7	44.8	70.2
16	14.2	393.5	89.6	6.7	26.3	44.8	68.1
17	26.0	475.5	120.6	10.7	22.4	40.4	62.5
18	10.6	450.1	129.8	11.0	22.0	39.5	64.3
19	23.9	450.5	77.8	5.5	28.3	47.0	67.4
20	12.1	402.6	98.7	19.1	16.4	40.2	68.4
21	12.4	358.7	48.5	2.5	35.4	53.0	72.3
22	19.9	354.7	66.9	8.1	26.0	49.0	72.8
23	30.3	358.6	78.7	5.4	28.4	47.0	71.0
24	35.0	369.1	77.5	3.0	31.2	47.5	70.5
25	35.4	396.1	108.2	12.5	21.1	41.2	67.4
26	23.8	359.7	92.1	7.6	25.4	44.6	70.8
27	25.4	395.4	117.1	21.3	15.3	37.9	66.9
28	31.9	385.2	66.6	2.1	37.4	49.6	68.9
29	25.5	342.5	80.4	7.1	26.4	46.5	71.5
30	26.7	388.6	97.4	6.7	26.3	44.1	68.1
31	31.0	337.2	66.6	1.6	29.6	49.1	69.9
32	23.1	386.4	67.2	5.2	36.9	49.5	72.3
33	25.6	364.4	62.6	1.8	35.0	50.1	70.5
34	25.8	382.9	77.4	1.8	34.3	48.2	68.6
35	28.1	405.5	85.0	8.5	24.7	44.8	68.1

The percentage passing at 14 mm (about the maximum size of the overburden fragments), which includes the fines fraction present in the block and the fines produced by the blast, is plotted versus the natural fines percentage in Fig. 16. Fractions passing at 63 and 250 mm are also plotted. Rewriting Eq. (3):

$$P(x) = P_L(x) \cdot \frac{100 - NF}{100} + NF, \tag{9}$$

$P_L(x)$ – the fragment sizes in the limestone, natural fines subtracted – is, ideally, only dependent on the blast design parameters, independent of the amount of natural fines; rearranging (9):

$$P(x) = P_L(x) + \left[1 - \frac{P_L(x)}{100}\right] NF, \tag{10}$$

i.e., $P(x)$ and NF are linearly related; linear fits are plotted for the three mesh sizes in Fig. 16. Although all linear fits have a positive slope, which is a general confirmation

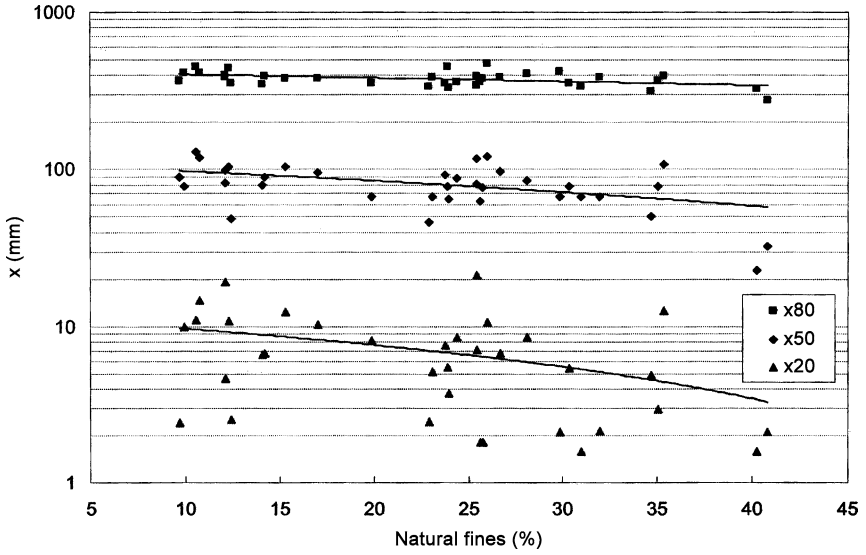

Fig. 15. Sensitiveness of the measurement system to the amount of fines; muckpile sizes for 80, 50 and 20% passing

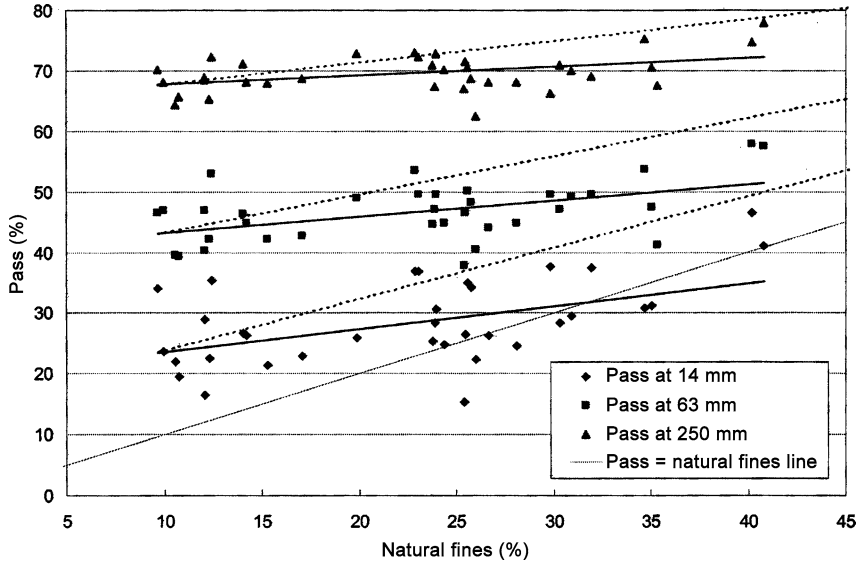

Fig. 16. Sensitiveness of the measurement system to the amount of fines; percentage passing at 14, 63 and 250 mm in the muckpile

that the system is sensitive to changes in the fragment sizes, many $P_{14\,\mathrm{mm}}$ values are unrealistic, as they are too close to the amount of natural fines, or even smaller. Both features are additional indications of the poor reliability of the results in the fines

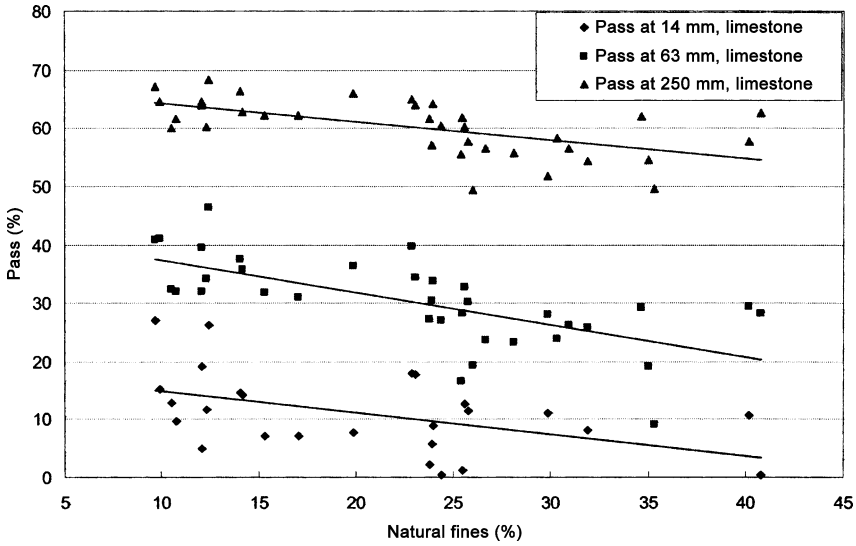

Fig. 17. Fragmentation in the limestone (natural fines subtracted). Spurious influence of the amount of natural fines

range, as discussed in Section 5. The larger scatter at smaller sizes can also be seen in this graph.

The trend lines in Fig. 16 are flatter than they should be – ideally, they should tend towards the (100, 100) point –. It appears that the image analysis handles the fines acceptably well for amounts of natural fines not too large, but that the fines are underestimated when they become abundant. This is more evident for blasts with natural fines fractions above 25%. This effect can also be seen in Fig. 17, where the fractions passing in the limestone (natural fines subtracted) which, according to the reasoning above, should be independent of the amount of natural fines, are plotted versus the natural fines; an apparent relation with the amount of natural fines appears for all fractions passing, which seem to decrease when the amount of natural fines increases. This is one more proof that the fines are underestimated in the measurements at high percentage of fines; after the natural fines are subtracted, the fine material turns to be less than real.

Considering the image analysis good in the low range of the amount of natural fines (the fines adjustment factor 110%, used in all blasts, was obtained for a blast with 10.8% natural fines), trend lines such as the dotted ones plotted in Fig. 16 – which pass through (100, 100) – should be expected. In order to achieve this, a variable fines adjustment factor has been defined in the following way:

Let $P^*_{14\,\mathrm{mm}}$ be the passing percentages whose linear regression function be the dotted line in Fig. 16; its equation is obtained as a straight line passing by the lower extreme of the original trend line (9.7, 23.5) and (100, 100):

$$(P^*_{14\,\mathrm{mm}})_{regr} = 15.3 + 0.85NF. \tag{11}$$

The individual $P_{14\,\mathrm{mm}}$ values are shifted to the $P^*_{14\,\mathrm{mm}}$ so that their relative positions about the Eq. (11) line are the same as their original positions about the original trend line. The images from each have were re-analyzed for this purpose with varying fines

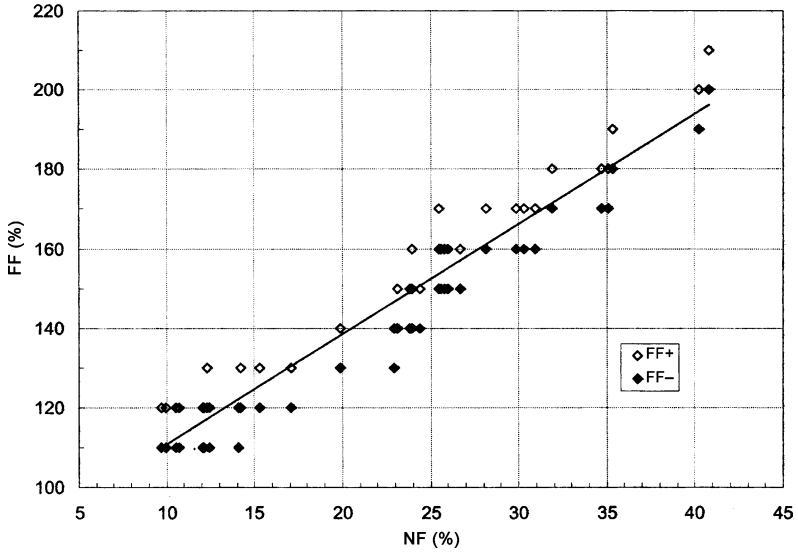

Fig. 18. Fines adjustment factor as a function of the amount of natural fines

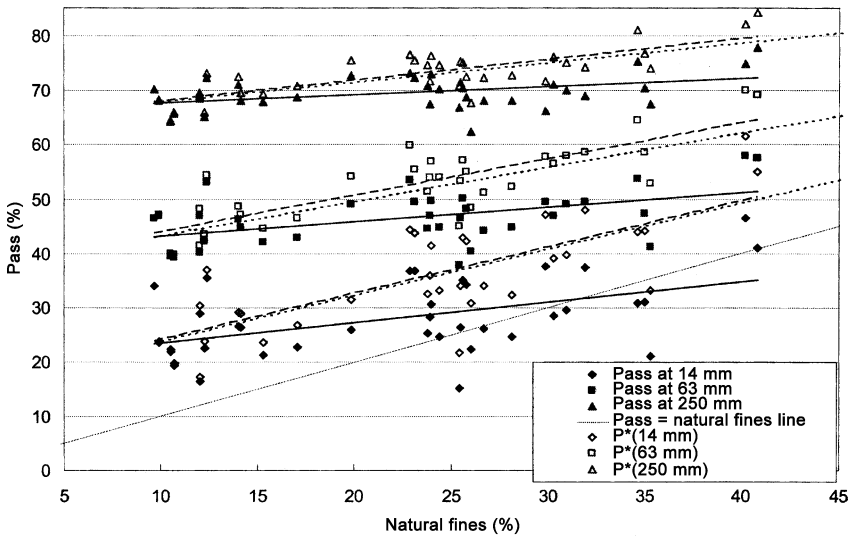

Fig. 19. Percentages passing at various sizes, muckpile. Solid points: constant FF; hollow points: variable FF. Solid lines: trend lines for constant FF; dotted lines: ideal trend lines; dashed lines: trend lines for variable FF

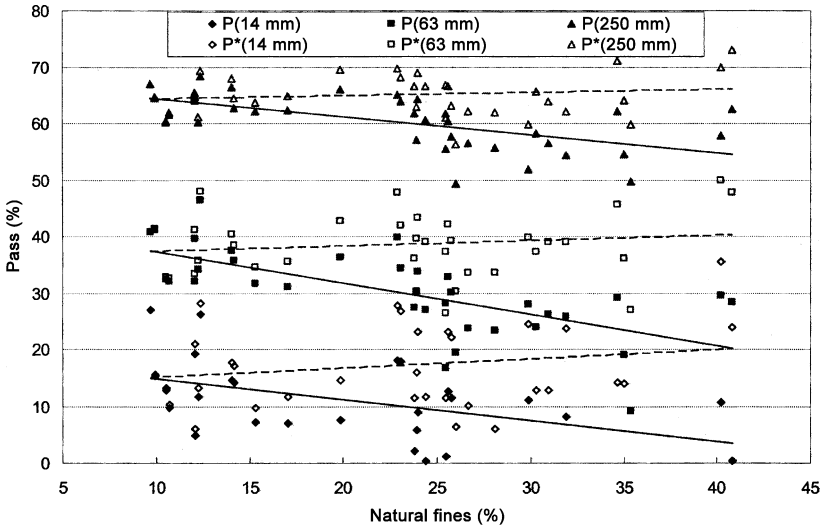

Fig. 20. Fragmentation in the limestone (natural fines subtracted). Solid lines: constant fines factor; dashed lines: variable fines factor

adjustment factor so that the passing value at 14 mm of the size distribution matches the calculated $P^*_{14\,\mathrm{mm}}$; FF increments of 10% were used, and the two consecutive values, FF_+ and FF_-, that bridge $P^*_{14\,\mathrm{mm}}$ were retained. They are shown in Fig. 18. A linear regression with $R^2 = 0.93$ has the equation:

$$FF = 83.0 + 2.77NF \tag{12}$$

The fragmentation curves are then recalculated with the fines factor from Eq. (12). The new passing percentages, $P^*_{14\,\mathrm{mm}}$, $P^*_{63\,\mathrm{mm}}$ and $P^*_{250\,\mathrm{mm}}$, are plotted in Fig. 19. The linear regression lines of P^* match quite well the expected ones (that for $P^*_{14\,\mathrm{mm}}$ is, naturally, almost coincident, as the $P_{14\,\mathrm{mm}}$ values were the ones used in the derivation of the fines factor function).

Figure 20 shows the percentage passing values at 14, 63 and 250 mm for the limestone, natural fines discounted. The spurious dependence (seen in the solid lines, the same as Fig. 17) of the fragmentation in the limestone with the amount of natural fines has now vanished.

7. Conclusions

The use of a digital image analysis system in a limestone quarry in which a loose overburden is blasted with the limestone rock has been thoroughly studied.

For the system to be effective, it was calibrated using screened data from a full scaled blast. The calibration was done setting the fines correction factor to a level where the image analysis output was as coincident as possible with the screened data.

The errors, either potential or real, and the limitations of the image analysis system, have been discussed; the following must be highlighted:

- Sample size. Twenty photographs per blast have been found to be an acceptable sample size when manual editing must be done. This amount is a compromise between the sample representativity and the cost of the analysis in person-hours; ten photographs may still do, though results are less reliable and more sample-dependent.
- Manual editing of the photographs has proved to be required in order to obtain acceptable results; such editing is carried out for about twenty minutes per photograph; longer time spending may not pay in terms of added accuracy of the size distribution curves. Manual editing of the images and correction of the particles, delineation cause errors due to the operator's limited visual sharpness and his personal skills; they tend to be larger at smaller particle sizes, well below the fines cut-off or the resolution of the image, but are limited at sizes larger than the optical resolution of the system.

The median of the absolute deviations about the median, a robust statistic applied to the median values of the size distributions of the photographs of each blast, has been used to detect outlier curves. The photographs so removed are replaced by new ones so that at least twenty photographs are used to form the total fragmentation curve.

The system operation aims at controlling the fragment size of the limestone from blasting. This requires the subtraction of the loose overburden material (natural fines) from the raw muckpile fragmentation curves. This has been done using laboratory screening data of the overburden material and the muckpile's fine fraction, together with the estimation of the natural fines fraction as the ratio of overburden thickness to bench height ratio.

The setup and operation of the system must be subject to careful analysis and control. Its absolute precision on a blast per blast basis is impossible to state in a production scenario. The sensitiveness of the system to the actual fragment size distribution has been checked by means of the known amount of fine material, of which a large portion comes from the overburden. A general consistency has been observed, though fines are more prone to be hidden in the analysis as they are more abundant. A fines adjustment factor adapted for a given amount of fines results too small to account for the fines if their amount is higher. A variable fines factor, linearly dependent with the amount of fines has been used to overcome this problem.

Acknowledgements

This work has been partially funded by the European Union, under the project ''Less Fines Production in Aggregates and Industrial Minerals industry'', contract no. G1RD-CT-2000-00438. We are indebted to the engineers Alberto Gómez and Javier Quemada of Cementos Portland Valderrivas for their enthusiasm and team work with the authors, and to Unión Española de Explosivos' technical services for their cooperation and long-term support. We would also like to thank Prof. Finn Ouchterlony of the Swedish Blasting Research Center (Swebrec) at the University of Luleå, and Prof. Peter Moser of the University of Leoben, for the valuable discussions and research cooperation.

References

Kemeny, J., Girdner, K., Bobo, T., Norton, B. (1999): Improvements for fragmentation measurement by digital imaging: Accurate estimation of fines. In: SAIMM (eds) Proc., 6th Int. Symposium for Rock Fragmentation by Blasting, Johannesburg, 103–109.

Latham, J. P., Kemeny, J., Maerz, N., Noy, M., Schleifer, J., Tose, S. (2003): A blind comparison between results of four image analysis systems using a photo-library of piles of sieved fragments, Int. J. Blasting Fragment. 7–2, 105–132.

Maerz, N. H., Zhou, W. (1998): Optical digital fragmentation measuring systems – inherent sources of error. Int. J. Blasting Fragment. 2(4), 415–431.

Miller, J. N., Miller, J. C. (2000): Statistics and chemometrics for analytical Chemistry. Prentice Hall, Harlow, UK, 172–175.

Moser, P. (2003): Less fines production in aggregate and industrial minerals industry. Proc., 2nd World Conference on Explosives and Blasting, Prague, 335–343.

Moser, P., Cheimanoff, N., Ortiz, R., Hochholdinger, R. (2000): Breakage characteristics in rock blasting. In: Proc., 1st World Conference on Explosives and Blasting Technique, Munich, 165–170.

Norton, B. (2003): Personal communication.

Ouchterlony, F. (2003): Influence of blasting on the size distribution and properties of muckpile fragments, a state-of-the art review. MinFo Project P2000-10; Energy optimisation in conminution. Swebrec, Luleå University of Technology, 81–95.

Ouchterlony, F. (2005): The Swebrec© function: linking fragmentation by blasting and crushing. Min. Technol. (Trans. Inst. Min. Metall. A) 114, 29–44

Rousseeuw, P. J., Leroy, A. M. (1987): Robust regression and outlier detection. Wiley, New York.

Split Engineering (2001): Split-Desktop Software Manual, Split Engineering LLC, Tucson.

Tessier, B., Schleifer, J., Grasedieck, A., Sanchidrián, J. A., Ouchterlony, F. (2002): Description and documentation of the fragmentation and blast data system installed in the quarries. Technical Report no. 12, Less Fines Project, E.U. contract G1RD-CT-2000-00438, École National Supérieure des Mines, Paris.

Author's address: Dr. J. A. Sanchidrián, Escuela Técnica Superior de Ingenieros de Minas (UPM), C/Rios Rosas 21, 28003 Madrid, Spain; e-mail: ja.sanchidrian@upm.es